# Robust Relationship Between Mid-latitudes CAPE and Moist Static Energy Surplus in Present and Future Simulations

Ziwei Wang[1] and Elisabeth Moyer[1]

[1]University of Chicago

May 25, 2023

## Abstract

Convective available potential energy (CAPE), a metric associated with severe weather, is expected to increase with warming, but we have lacked a framework that describes its changes in the populated midlatitudes. In the tropics, theory suggests mean CAPE should rise following the Clausius-Clapeyron (C-C) relationship at ~6%/K. In the heterogeneous midlatitudes, where the mean change is less relevant, we show that CAPE changes are larger and can be well-described by a simple framework based on moist static energy (MSE) surplus, which is robust across climate states. This effect is highly general and holds across both high-resolution nudged regional simulations and free-running global climate models. The simplicity of this framework means that complex distributional changes in future CAPE can be well-captured by a simple scaling of present-day data using only three parameters.

# Robust Relationship Between Midlatitudes CAPE and Moist Static Energy Surplus in Present and Future Simulations

**Ziwei Wang**[1,2], **Elisabeth J. Moyer**[1,2]

[1]Department of the Geophysical Sciences, University of Chicago, Chicago, Illinois
[2]Center for Robust Decision-making on Climate and Energy Policy (RDCEP), University of Chicago, Chicago, Illinois

**Key Points:**

- In midlatitudes summer, future CAPE increases show distributional structure and it is insufficient to be described with mean changes
- CAPE shows a strong dependence on "MSE surplus" and this dependence holds across climate states
- The CAPE distributional shift is well captured by adjusting current climate profiles with 3 parameters: surface T and RH, and upper-level T

Corresponding author: Elisabeth Moyer, `moyer@uchicago.edu`

## Abstract

Convective available potential energy (CAPE), a metric associated with severe weather, is expected to increase with warming, but we have lacked a framework that describes its changes in the populated midlatitudes. In the tropics, theory suggests mean CAPE should rise following the Clausius–Clapeyron (C–C) relationship at ∼6%/K. In the heterogeneous midlatitudes, where the mean change is less relevant, we show that CAPE changes are larger and can be well-described by a simple framework based on moist static energy (MSE) surplus, which is robust across climate states. This effect is highly general and holds across both high-resolution nudged regional simulations and free-running global climate models. The simplicity of this framework means that complex distributional changes in future CAPE can be well-captured by a simple scaling of present-day data using only three parameters.



## Plain Language Summary

Severe thunderstorms cause substantial damage and may become more destructive in the future. Because these events are associated with conditions of high "Convective Available Potential Energy" (CAPE), it is important to understand how CAPE might increase in a future warmer climate, but existing theories designed for the tropics are not suitable for the U.S. and similar areas. We find that future changes in CAPE are complex and cannot be predicted based on surface temperature alone, but can be using three factors: temperature and moisture at the surface and temperature at a higher level. A single simple framework is able to explain CAPE differences between present and future, warm and cold regions, or daytime and nighttime.


## 1 Introduction

Convective Available Potential Energy (CAPE), loosely defined as the vertically integrated buoyancy of a near-surface air parcel, is a metric closely associated with extreme convective weather events that can cause substantial socioeconomic damages (e.g., Johns & Doswell, 1992). CAPE is derived from the difference between the temperature profile of a parcel rising pseudo-adiabatically from the surface and that of the background environment (Moncrieff & Miller, 1976), which determines the maximum possible updraft velocity during undiluted ascent. In meteorology, CAPE is used to predict thunderstorm events and in particular hail (Groenemeijer & van Delden, 2007; Kunz, 2007; Kaltenböck et al., 2009). Studies have also used the covariate of CAPE and wind shear to explain differences in thunderstorm frequency across locations (Brooks et al., 2003, 2007) or across climate states (Trapp et al., 2009; Diffenbaugh et al., 2013).

Early efforts to understand CAPE in observations sought to characterize it as a function of near-surface temperature and moisture (Williams & Renno, 1993; Ye et al., 1998). More recent studies of CAPE in observations have tended to focus on decadal-scale trends, often finding large increases. For example, (Gettelman et al., 2002) found trends equivalent to ∼50%/K in 15 tropical radiosonde stations. Model studies of CAPE under climate change have tended to produce smaller effects. Several recent studies that simulate the tropics using convection-permitting models (0.2–4 km resolution) without advection, i.e. approximating radiative-convective equilibrium, find CAPE increases of 8%/K (Muller et al., 2011), 8%/K (Romps, 2011), 12%/K (Singh & O'Gorman, 2013), 7%/K (Seeley & Romps, 2015), and 6–7%/K from theory (Romps, 2016). In the midlatitudes, changes may be larger: both Diffenbaugh et al. (2013) and Chen et al. (2020) show ∼10%/K over the Eastern part of the continental United States. The representation of CAPE changes is extensively evaluated across CMIP6 models by Lepore et al. (2021), finding 10–14%/K changes for U.S. and 6–8%/K changes for regions including Europe, India and Southeast Asia.

Theoretical frameworks to explain climatological CAPE fall into two groups. One approach assumes that background environmental profiles are fully determined by surface temperature, and predicts them by considering the effects of convective entrainment. Singh and O'Gorman (2013) proposed a "zero-buoyancy model" based on the assumption that entrainment makes actual buoyancy in an ascending convective plume small relative to CAPE (with column RH considered fixed). Singh and O'Gorman (2015) and Zhou and Xie (2019) extended the work and validated the approach under radiative-convective equilibrium (RCE). However, the theory is not expected to work for midlatitudes land, which has strong spatial and temporal variations, even though its climatological mean profile is close to RCE (Miyawaki et al., 2022).

A second approach treats surface and mid-tropospheric conditions as independent variables. Emanuel and Bister (1996) (henceforth EB96) drew on heat engine theory and described the relationship as

$$CAPE \ = \ A \cdot (h_s - h_m) \tag{1}$$

where $h_s$ and $h_m$ are moist static energy (MSE) near the surface (boundary layer) and in the mid-troposphere, respectively. In this perspective, CAPE represents the maximum possible kinetic energy that can be released given a heat transfer of ($h_s - h_m$), and CAPE is generated only when surface MSE exceeds that of a mid-tropospheric threshold. Agard and Emanuel (2017), Li and Chavas (2021) (hereafter, AE17 and LC21) and Chavas and Li (2022) modified the approach to use a different threshold term, dry static energy, and showed that results captured aspects of CAPE variations in the midlatitudes.

We modify the framework based on Emanuel (1994) and use as the threshold term the minimum "saturation MSE" $h_m^*$ in the mid-troposphere, the moist static energy a parcel would have if saturated:

$$CAPE = A \cdot (h_s - h_m^*) \tag{2}$$

We term the difference $h_s - h_m^*$ the 'MSE surplus'. The integral form of this expression can be derived from the definition of CAPE given the assumption that the effect of water vapor on buoyancy is negligible. (See Supporting Information Text S1.) We then simplify to a linear dependence (as in e.g. AE17) by replacing the integral with a difference at a single location. This assumption is valid as long as the shape of the environmental temperature profile does not vary strongly with $h_s$ and can be folded into the slope $A$. The rationale for $h_m^*$ as the threshold term can also be expressed intuitively: CAPE depends only on temperature differences, and above the level of free convection, the rising parcel is saturated and conserves $h^*$, so its difference with the environment should be taken with a comparable quantity. Zhang and Boos (2023) used $h_m^*$ as a threshold for convective instability over summertime mid-latitude land, but Equation (2) has not yet been evaluated as a framework for CAPE.

A sufficiently general framework should explain not only average CAPE, or CAPE in the average profile, but its variations across space and time in the highly heterogeneous midlatitudes. This generality is required for any application to extreme weather, since only the high tail of CAPE is associated with the severe thunderstorms that produce large socioeconomic impacts. Although no prior work has addressed future changes in midlatitudes CAPE distributions, studies suggest they may shift in complex ways. For example, Chen et al. (2020) show that spatial patterns of CAPE changes over North America differ from those of present-day CAPE.

In this work, we use observations and model simulations to evaluate how CAPE changes under $CO_2$-induced warming, and to test whether the relationship of Equation (2) captures these changes. That is, we ask whether it robustly applies to current and future CAPE distributions across climate states. Furthermore, we ask whether robustness means that complex distributional changes can be reproduced by as few as three parameters derived from regional means. Our goal is to quantify changes in CAPE distributions in the midlatitudes and to provide a simple framework that explains them.

## 2 Data and Methods

### 2.1 Model output

Most analysis here uses high-resolution model output: a paired set of present and future dynamically downscaled simulations over continental North America from the Weather Research and Forecasting model (WRF, version 3.4.1) run at 4 km resolution. Both runs are described in Liu et al. (2017) and are acquired from NCAR RDA (Rasmussen & Liu, 2017). The present-day simulation (CTRL) uses ERA-Interim reanalysis for initial and boundary conditions and for a large-scale spectral nudging (scales >2000 km) applied to levels above the planetary boundary layer, to match planetary-scale weather patterns. Small-scale processes can still evolve freely. The future simulation is a pseudo-global-warming (PGW) scenario, treated identically but with reanalysis adjusted by a spatially- and temporally-varying offset derived from the CMIP5 multi-model mean projection under RCP8.5, to reflect large-scale changes under increased $CO_2$. These runs have been validated against observations (Wang et al., 2021) and used in studies of future CAPE changes (Sun et al., 2016; K. L. Rasmussen et al., 2017). In this work, we use the years 2001–2012 and the equivalent future period.

To test whether results apply generally to a diverse set of free-running models, we use 11 CMIP6 models, selected based on the availability of the 6-hourly output needed for CAPE calculation. Model biases range from -60–+1700 J/kg, with the best performance (MPI-ESM1-2-LR) comparable to WRF, at ∼30 vs. 14 J/kg (Wang et al., 2021; Chavas & Li, 2022). We use pairs of historical (2005-2014) and ssp585 (2091-2100) simulations (Eyring et al., 2016). To allow comparison with observations, we subset all model output to 80 grid points that match International Global Radiosonde Archive (IGRA) weather stations in North America, as in Wang et al. (2021). For consistency, we calculate surface-based CAPE in all runs using the same python package. For 'paired' comparisons, we match each profile in CTRL/historical with its equivalent in PGW/ssp585. As in prior studies, most analyses here use only the summertime (MJJA or JJA), when convection is most active.

### 2.2 Methods: regressions and subsetting

All linear fits in this work are made using binned median data, to homogenize CAPE sampling. All fits are computed using orthogonal distance regression (ODR), which is most appropriate in conditions where errors in both dependent and independent variables matter. See Schwarzwald et al. (2021) for discussion of ODR. When fitting to estimate the fractional change in CAPE between climate states, we use the entire dataset, and we divide by the overall mean temperature change (4.65 K in WRF runs) when giving values in %/K. However, many comparisons focus on convective conditions and therefore involve a subset of the data. For regressions of CAPE against MSE surplus, we impose an absolute cut at CAPE >1000 J/kg. In other cases we compute values for profiles above the 73rd quantile in CAPE, which corresponds to CAPE >1000 J/kg in the WRF CTRL run. When constructing synthetic profiles, we apply a temperature offset derived from profiles with CAPE >73rd percentile in each climate state (3.92 K in WRF runs), to best capture the change in convective conditions.

### 2.3 Synthetic profiles

To help understand the minimal information needed to reproduce future CAPE changes, we construct three synthetic CAPE distributions based on the WRF CTRL profiles.

1. For *Clausius-Clapeyron* scaling, shown for illustrative purposes only, we simply multiply each CTRL CAPE value by 1.33 ($= e^{0.061 \cdot 4.65}$, where 6.1%/K is C–C for the mean temperature of high-CAPE profiles, 301.8 K). We neglect several factors whose systematic effects on CAPE would largely cancel: the projected rise in the Level of Neutral Buoyancy (LNB) (+0.6%/K); the reduction in surface RH (-0.4%/K), and treating profiles separately (-0.1%/K).
2. For the *constant offset* case, we add a fixed temperature offset of 3.92 K to each CTRL profile at each level from surface to 200 hPa (near the LNB in the mean CTRL profile), then linearly interpolate to zero change at 75 hPa. We show cases with and without a surface RH adjustment of -0.9%, the mean change for profiles with CAPE >73rd quantile.
3. For the *lapse rate adjustment* case, we modify the *constant offset* procedure to also include a change in lapse rate $\Gamma = (T_s - T_{200})/z_{200}$. That is, we linearly interpolate between a warming of 3.92 K at the surface and a similarly-derived 4.94 K at 200 hPa. We apply the -0.9% surface RH adjustment.

For context, we also show predictions of the SO13 theory under a 4.65 K temperature rise. We derive entrainment rate parameters of 0.67 and 0.68 for the WRF CTRL and PGW runs, and use LNB values for each profile. (Singh and O'Gorman (2013) used a fixed entrainment parameter of 0.75 and a fixed LNB temperature of 200 K.)

## 3 Results

### 3.1 Changes in CAPE distributions

We begin our analysis by asking: in midlatitudes model projections, how much and how does CAPE change with warming? In the WRF model runs, average summertime CAPE rises by 10% per degree of warming (a 61% increase, from 684 to 1103 J/kg with a mean surface temperature rise of 4.65 K). However, an alternate approach that emphasizes changes in higher-CAPE conditions may be more appropriate, and we use it throughout this work. We perform an orthogonal regression on the density distributions of paired profiles in present and future runs, which yields a clear shift upwards even though weather systems are not identical in the two runs and the scatter is therefore large (Figure 1, left). The slope yields a CAPE increase of 8.0%/K (45% total). With either method, the change is larger than in Clausius Clapeyron (6.1%/K) or in the SO13 theory developed for the tropics (6.0%/K), but smaller than would result from simply changing surface values while leaving atmospheric profiles unchanged (11.7%/K in the *constant offset* synthetic, which adds a single $\Delta$T to all levels in all profiles). (See Figure S2.) Midlatitudes atmospheric lapse rates have therefore lessened slightly in the future simulation, as expected.

Distributional effects in future CAPE changes can be readily seen by comparing values for individual quantiles to the overall regression line (Figure 1, left, dots). The lower quantiles lie above the regression line and the extreme high-CAPE quantiles (>∼3000 J/kg) below it, meaning the future CAPE distribution is narrower than that produced by a simple mean shift. This relative narrowing manifests as a downward slope in a quantile regression plot, which shows the ratio of individual quantiles of future vs. present-day CAPE (Figure 1, right). The effect is a necessary result of the nonlinear CAPE - temperature relationship: a given temperature rise produces a greater effect in low-CAPE conditions. For this reason, relative narrowing occurs even when surface temperature increases are uniform and environmental profiles do not change (*constant offset*, green) or

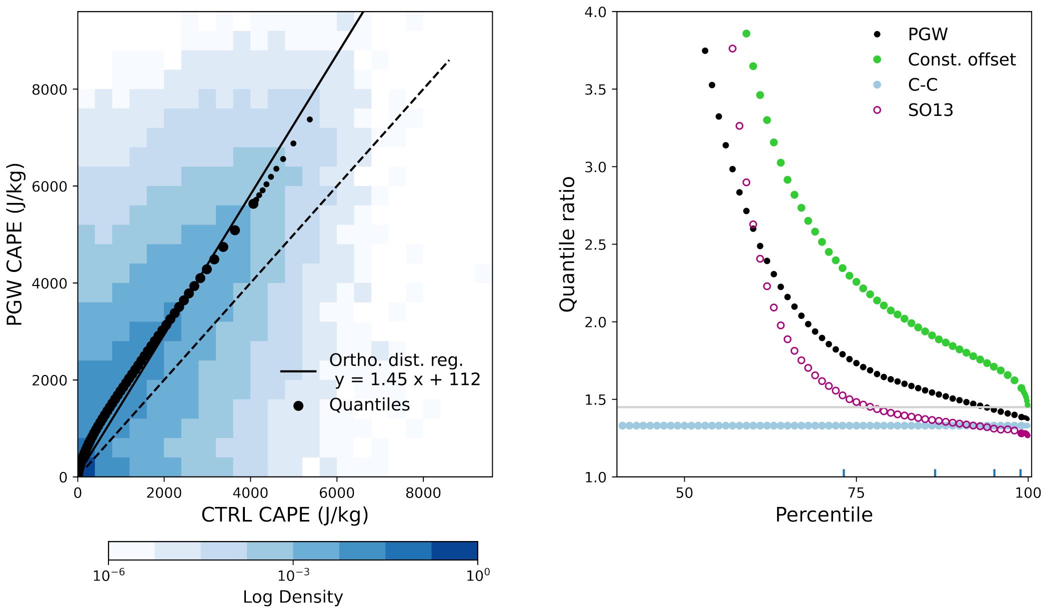


**Figure 1.** (Left) Comparison of CAPE in present (CTRL) and future (PGW) model runs as a density plot of paired profiles (see Methods), showing also the 1:1 line (dashed); the orthogonal regression (solid); and quantiles of the distribution (large dots, 1% increments from 0-0.99; small dots 0.1% increments above 0.99). (Right) Quantile ratio plot, constructed by taking the ratio of future to present CAPE quantiles, showing WRF output (black, same dots as L. panel), the synthetic datasets *C-C scaling* (light blue) and *constant offset* (green), and for reference *SO13* (purple, with changes computed relative to its own CTRL distribution). Gray horizontal line marks the +45% mean change from the orthogonal regression. Four vertical tick bars mark the percentiles matching 1000, 2000, 3000, and 4000 J/kg (73.2%, 86.5%, 95.1%, and 98.9%, respectively). The x-axis is truncated to omit quantiles where CTRL CAPE is zero. Changes in WRF are smaller than those in *constant offset*, implying some lapse rate adjustment.

in a theoretical approach that does not use observed environmental profiles (SO13, purple).

### 3.2 The effect of changes in environmental profiles

We found in section 3.1 that environmental adjustments appear to reduce future CAPE increases. To isolate this effect, we examine mean CAPE in surface temperature and humidity (T–H) space, following Wang et al. (2021) (Figure 2). Since surface T and H uniquely define the moist adiabat on which a parcel rises, a change in CAPE for a given T–H is due only to an altered environmental profile. This approach effectively decomposes CAPE changes into a sampling effect and a partially compensating lapse rate effect. In the WRF model runs used here, increased sampling of hot and humid surface conditions in PGW would more than double CAPE from its CTRL values if environmental profiles remained constant (Figure 2, top), but environmental changes nearly halve that increase (Figure 2, bottom). This environmental damping makes future CAPE smaller for each T–H bin, so that hotter or wetter surface conditions are needed to achieve the same CAPE.

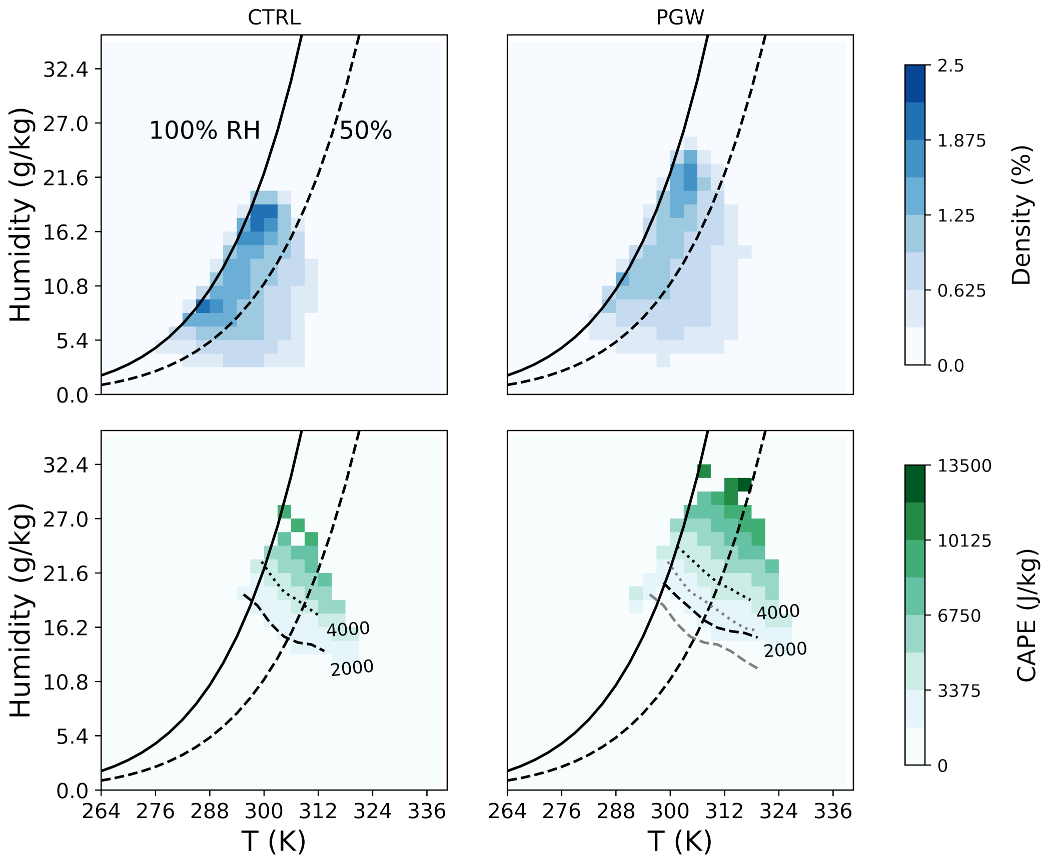


**Figure 2.** Density heatmaps of (top) sampling of T–H bins and (bottom) mean CAPE in each T–H bin, in CTRL (left) and PGW (right) WRF runs during summer (MJJA). Bins shown are all those with 3 or more observations. Solid and dashed lines mark RH of 100 and 50%. In the bottom row, dashed/dotted lines mark CAPE contours at 2000 and 4000 J/kg, with CTRL contours repeated in PGW panel as gray lines. Although conditions sampled in PGW are hotter than in CTRL (top), each given T,H bin is associated with smaller CAPE (bottom).

Most of this damping results from subtle changes in environmental profiles. Lapse rates across the domain lessen by 3% between CTRL and PGW, from -6.56 to -6.35 K/km (for the CAPE >73rd quantile subset). However, some damping also occurs even if the lapse rate distribution remains fixed (Figure S3). Because lapse rates in our domain are correlated with temperature – binned averages range from -5 K/km at 270 K to over -7 K/km at 320 K – then as the surface warms, each given temperature become associated with more stable conditions (Figure S4). The combined result is that CAPE contours in T–H space shift substantially between CTRL and PGW.

We can immediately make two inferences about CAPE changes in our model runs. First, because CAPE contours align with those of MSE (Figure S5), CAPE in our dataset must be strongly related to surface MSE. Second, because CAPE contours in T–H space shift while MSE by definition cannot, this relationship must shift in future simulations. Both effects are consistent with Equation (2).

### 3.3 CAPE-MSE surplus framework

As predicted, the relationship between CAPE and surface MSE is reasonably linear in each climate state and shifts as the climate warms (Figure 3, top left). That is, CAPE on average does not develop unless surface MSE ($h_s$) exceeds some threshold, which changes between present and future simulations. This threshold, the x-intercept of the fitted regression, matches the mean minimum saturation MSE ($h_m^*$) in each climate state to within $< 0.3\%$. When CAPE is plotted against MSE surplus ($h_s - h_m^*$) instead, as in Equation (2), the relationship becomes robust across climate states and the residual variance becomes smaller, suggesting that this is a fundamental physical relationship (Figure 3, top right). On both measures, variance and robustness, the CAPE-MSE surplus relationship of Equation (2) outperforms the expression based on dry static energy used in Agard and Emanuel (2017) and Li and Chavas (2021) (Figure S6, which shows both WRF runs and observations). Fitted slopes are nearly identical in WRF CTRL and PGW runs and in observations (0.27 in all), and intercepts are nearly zero (0.7, 1.1, and 1.6 kJ/kg for CTRL, PGW, and observations, respectively). In this perspective, the effects of climate change reduce to a greater sampling of conditions with high MSE surplus.

The relationship described by Equation (2) applies across all models tested and appears remarkably robust not only across climate states but across locations and times. It holds in 11 free-running climate models from the CMIP6 archive (Figure 3, bottom), though they differ strongly in their CAPE distributions and projected changes: mean values over present-day summertime N. America range from 704 to over 2461 J/kg, and future changes range from 5-10%/K. Their CAPE-MSE surplus relationships also differ, with slopes of 0.22 to 0.29. Nevertheless, in each model that relationship remains constant across climate states. In the WRF model output, fitted slopes to CAPE vs. MSE surplus remain similar when the dataset is divided by latitude (northern vs. southern stations), by time of day (daytime vs. nighttime profiles), by interannual variations (anomalously warm vs. cold years), or even by season (winter vs. summer) (Figure S7).

### 3.4 A 3-parameter transformation

The robustness of Equation (2) across climate states suggests that model-projected CAPE changes result from relatively simple adjustments. The fitted slope for each model, $A$, is a function of the shape of the environmental profile; for $A$ to remain constant, that shape must not alter much. Changes in CAPE in Equation (2) can then result only from changes in surface conditions ($h_s$, which depends on surface temperature and humidity), or in a single metric of temperature in the free troposphere ($h_m^*$). While the quantile ratio plot in Figure 1 shows that transformations based on 1 or 2 parameters are insufficient for describing CAPE distributional changes, it appears that 3 parameters may be sufficient.

To construct our scaling, we use the two effects that produce the shift in CAPE contours in T–H space seen in Section 3.2 – an overall surface warming and a small decrease in mean lapse rates – and add the small but significant change in surface relative humidity in our WRF runs (-0.9%). As described in Methods, we calculate mean changes in these three parameters across our domain and apply them to the CTRL profiles. This simple adjustment correctly produces the shifting CAPE-MSE relationship, matching its slope and x-intercept (Figure 4, left). It also reproduces both the distributional narrowing and the magnitude of CAPE change for the high-CAPE conditions of interest (Figure 4, right). While midlatitudes CAPE is highly heterogeneous, a relatively straightforward transformation can capture its full distributional change in a future warmer climate.

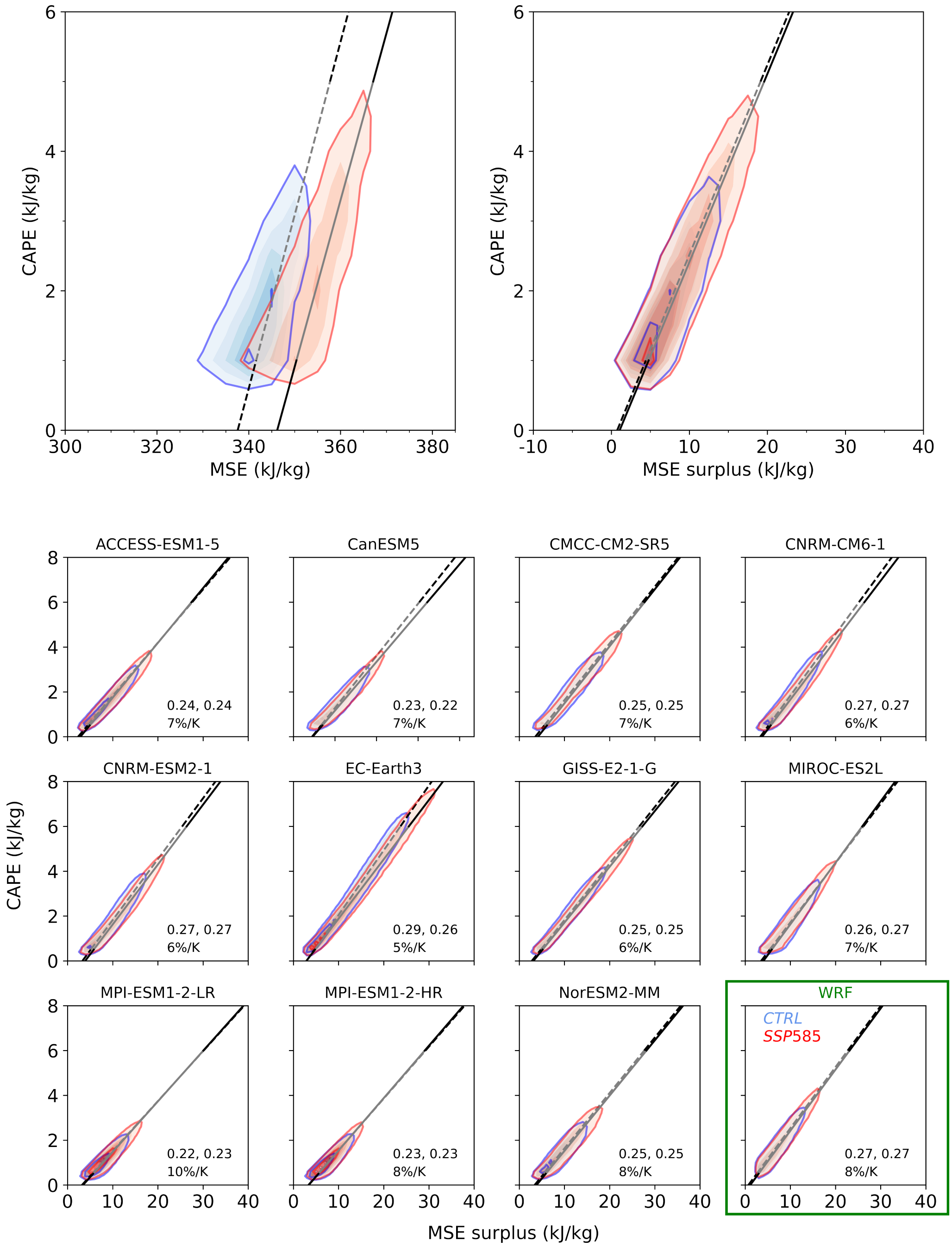


**Figure 3.** (Top) Relationships between CAPE and surface MSE (left) and MSE surplus (right), for WRF runs in in N. America summertime (MJJA), showing all cases where CAPE >1000 J/kg (CTRL = blue, dotted; PGW = red, solid). Lines are fitted orthogonal regressions. Color shading increments are 1.5% for the left panel and 0.75% for the right. The CAPE-MSE surplus relationship is robust across climate states. (Bottom) CAPE–MSE surplus relationships in 11 free-running CMIP6 models and WRF for N. American summertime (JJA), using all cases where CAPE >500 J/kg. Color shading increments are 0.5% for all models except EC-Earth3 (0.25%). The CAPE–MSE surplus is robust in all models, even those with with unrealistic CAPE.

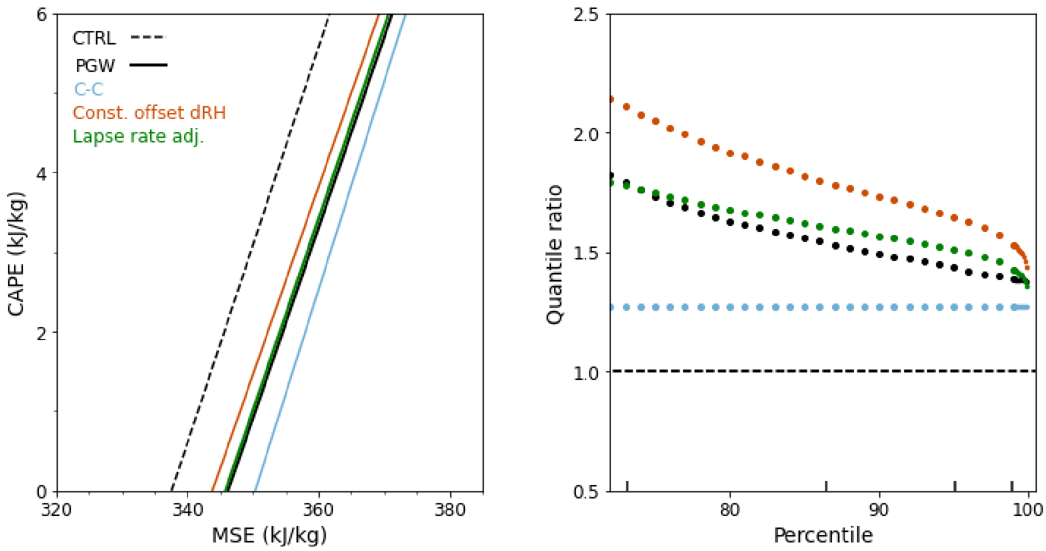


**Figure 4.** Comparison of present and future CAPE in model output (black) and synthetics: *C–C scaling* (light blue), *constant offset* including an RH adjustment (orange), and *lapse rate adjustment* (green). (Left) Fitted regression lines of the future CAPE-MSE relationship as in Figure 3. See Table S1 for slopes and x-intercepts. (Right) Future changes in CAPE as quantile ratio plots, as in Figure 1. The simple *lapse rate adjustment* effectively reproduces CAPE distributional changes.

## 4 Discussion

Increases in severe weather events, which are associated with high CAPE, are a substantial societal concern under global warming. Their understanding has been hindered by lack of a widely accepted theory or framework to describe midlatitudes CAPE changes. Theories developed for the convective tropics (e.g. Singh & O'Gorman, 2013), are not appropriate for midlatitudes land, where advection and a strong diurnal cycle mean that the mid-troposphere is often decoupled from the surface (Figure S9). In this work, we show that Equation (2), a modified version of the heat-engine theory originally proposed in 1996 (EB96) and of its later extensions (AE17, LC21), provides a compact representation of midlatitudes CAPE that is robust across space, over diurnal and seasonal cycles, and across climate states.

We term the work developed here a framework rather than a theory because the transformation requires empirical values and we do not predict the slope $A$, which accounts for the shape of the environmental profile and is empirically fit. Similarly, AE17 would require an empirical correction to their slope $ln(T_i/T_n)$ for a realistic moist atmosphere. In EB96, by contrast, $A$ is based on thermodynamics and is effectively the Carnot efficiency of the atmosphere. In our WRF runs, the empirical slope of the CAPE-MSE relationship is larger than Carnot (0.24, vs. 0.14 for Carnot as defined by EB96), but this is not a violation of the 2nd Law given our focus on highly convective conditions.

Any transformation that describes changes in midlatitudes CAPE will necessarily require at least three parameters, one more than SO13, because the midlatitudes free troposphere cannot be predicted from surface T and RH even on average. In this work we find that *only* three parameters are required: three regional mean values across our domain are sufficient to capture the full distributional change in the CAPE >73rd quantile. This result may seem counterintuitive, since present-day North America encompasses a wide range of environmental conditions, future climate changes are spatially variable, and the response of CAPE is highly nonlinear. However, CAPE develops appreciably only in a relatively restricted subset of T–H space, where changes are more uniform.

The CAPE changes projected in our WRF runs and in most CMIP6 models are higher than Clausius-Clapeyron, the expectation under RCE. This difference matters for occurrence of extreme conditions. Incidences of summertime CAPE >2000 J/kg, a commonly-used threshold for severe weather, rise half again as much in our WRF projections as under C–C scaling (14% in CTRL; >24% in PGW, 20% in *C–C*). Predicting how these extreme values will affect future severe weather requires also understanding how they will map to convective updraft velocities, but understanding CAPE changes under $CO_2$-induced warming is a necessary first step. The dependence of CAPE on MSE surplus provides a simple but robust framework for predicting and understanding that response.

## Data Availability Statement

The 4-km WRF Convection-permitting model output is downloaded from NCAR RDA (`https://rda.ucar.edu/datasets/ds612.0/`). The IGRA radiosonde data is downloaded from NOAA (`https://www.ncei.noaa.gov/products/weather-balloon/integrated-global-radiosonde-archive`). CMIP6 model output are acquired from Earth System Grid Federation (ESGF, `https://esgf-node.llnl.gov/projects/cmip6/`).

**Acknowledgments**
The authors thank Dan Chavas, Tiffany Shaw, Funing Li, Zhihong Tan, and Osamu Miyawaki for constructive comments, and the National Center for Atmospheric Research (NCAR) for providing the WRF dataset. We acknowledge the World Climate Research Programme, which, through its Working Group on Coupled Modelling, coordinated and promoted CMIP6. We thank the climate modeling groups for producing and making available their model output, the Earth System Grid Federation (ESGF) for archiving the data and providing access, and the multiple funding agencies who support CMIP6 and ESGF. This work is supported by the Center for Robust Decision-making on Climate and Energy Policy (RDCEP), funded by the NSF Decision Making Under Uncertainty program, Award SES-1463644, and was completed in part with resources provided by the University of Chicago Research Computing Center.

## References

Agard, V., & Emanuel, K. (2017). Clausius–Clapeyron scaling of peak CAPE in continental convective storm environments. *Journal of the Atmospheric Sciences*, *74*(9), 3043–3054. doi: 10.1175/JAS-D-16-0352.1

Brooks, H. E., Anderson, A. R., Riemann, K., Ebbers, I., & Flachs, H. (2007). Climatological aspects of convective parameters from the NCAR/NCEP reanalysis. *Atmospheric Research*, *83*(2), 294–305. doi: 10.1016/j.atmosres.2005.08.005

Brooks, H. E., Lee, J. W., & Craven, J. P. (2003). The spatial distribution of severe thunderstorm and tornado environments from global reanalysis data. *Atmospheric Research*, *67-68*, 73–94. doi: 10.1016/S0169-8095(03)00045-0

Chavas, D. R., & Li, F. (2022). Biases in cmip6 historical u.s. severe convective storm environments driven by biases in mean-state near-surface moist static energy. *Geophysical Research Letters*, *49*(23), e2022GL098527. doi: https://doi.org/10.1029/2022GL098527

Chen, J., Dai, A., Zhang, Y., & Rasmussen, K. L. (2020). Changes in convective available potential energy and convective inhibition under global warming. *Journal of Climate*, *33*(6), 2025 - 2050. doi: 10.1175/JCLI-D-19-0461.1

Diffenbaugh, N. S., Scherer, M., & Trapp, R. J. (2013). Robust increases in severe thunderstorm environments in response to greenhouse forcing. *PNAS*, *110*(41), 16361–16366. doi: 10.1073/pnas.1307758110

Emanuel, K. (1994). Atmospheric Convection, Chap. 6. In (pp. 169–175). Oxford Univ. Press.

Emanuel, K., & Bister, M. (1996). Moist convective velocity and buoyancy scales. *J. Atmos. Sci.*, *53*(22), 3276–3285. doi: 10.1175/1520-0469(1996)053⟨3276:MCVABS⟩2.0.CO;2

Eyring, V., Bony, S., Meehl, G. A., Senior, C. A., Stevens, B., Stouffer, R. J., & Taylor, K. E. (2016). Overview of the coupled model intercomparison project phase 6 (CMIP6) experimental design and organization. *Geoscientific Model Development*, *9*(5), 1937–1958. doi: 10.5194/gmd-9-1937-2016

Gettelman, A., Seidel, D. J., Wheeler, M. C., & Ross, R. J. (2002). Multidecadal trends in tropical Convective Available Potential Energy. *Journal of Geophysical Research: Atmospheres*, *107*, ACL 17–1–ACL 17–8. doi: 10.1029/2001JD001082

Groenemeijer, P. H., & van Delden, A. (2007). Sounding-derived parameters associated with large hail and tornadoes in the netherlands. *Atmospheric Research*, *83*(2), 473–487.

Johns, R. H., & Doswell, I., Charles A. (1992). Severe local storms forecasting. *Weather and Forecasting*, *7*(4), 588-612. doi: 10.1175/1520-0434(1992)007⟨0588:SLSF⟩2.0.CO;2

Kaltenböck, R., Diendorfer, G., & Dotzek, N. (2009). Evaluation of thunderstorm indices from ECMWF analyses, lightning data and severe storm reports. *Atmospheric Research*, *93*(1), 381–396. doi: 10.1016/j.atmosres.2008.11.005

Kunz, M. (2007). The skill of convective parameters and indices to predict isolated and severe thunderstorms. *Natural Hazards and Earth System Sciences*, *7*(2), 327–342.

Lepore, C., Abernathey, R., Henderson, N., Allen, J. T., & Tippett, M. K. (2021). Future Global Convective Environments in CMIP6 Models. *Earth's Future*, *9*(12), e2021EF002277. doi: 10.1029/2021EF002277

Li, F., & Chavas, D. R. (2021). Midlatitude continental CAPE is predictable from large-scale environmental parameters. *Geophysical Research Letters*, *48*(8), e2020GL091799. doi: 10.1029/2020GL091799

Liu, C., Ikeda, K., Rasmussen, R., Barlage, M., Newman, A. J., Prein, A. F., … Yates, D. (2017). Continental-scale convection-permitting modeling of the current and future climate of north america. *Clim Dyn*, *49*(1), 71–95. doi: 10.1007/s00382-016-3327-9

Miyawaki, O., Shaw, T. A., & Jansen, M. F. (2022). Quantifying energy balance regimes in the modern climate, their link to lapse rate regimes, and their response to warming. *Journal of Climate*, *35*(3), 1045 - 1061. doi: 10.1175/JCLI-D-21-0440.1

Moncrieff, M. W., & Miller, M. J. (1976). The dynamics and simulation of tropical cumulonimbus and squall lines. *Quarterly Journal of the Royal Meteorological Society*, *102*(432), 373–394. doi: 10.1002/qj.49710243208

Muller, C. J., O'Gorman, P. A., & Back, L. E. (2011). Intensification of precipitation extremes with warming in a cloud-resolving model. *J. Climate*, *24*(11), 2784–2800. doi: 10.1175/2011JCLI3876.1

Rasmussen, & Liu, C. (2017). *High resolution WRF simulations of the current and future climate of North America.* Research Data Archive at the National Center for Atmospheric Research, Computational and Information Systems Laboratory. (accessed 30 Oct 2019, `https://doi.org/10.5065/D6V40SXP`)

Rasmussen, K. L., Prein, A. F., Rasmussen, R. M., Ikeda, K., & Liu, C. (2017). Changes in the convective population and thermodynamic environments in convection-permitting regional climate simulations over the united states.

*Climate Dynamics*. doi: 10.1007/s00382-017-4000-7

Romps, D. M. (2011). Response of tropical precipitation to global warming. *J. Atmos. Sci.*, *68*(1), 123–138. doi: 10.1175/2010JAS3542.1

Romps, D. M. (2016). Clausius–Clapeyron scaling of CAPE from analytical solutions to RCE. *Journal of the Atmospheric Sciences*, *73*(9), 3719-3737. doi: 10.1175/JAS-D-15-0327.1

Schwarzwald, K., Poppick, A., Rugenstein, M., Bloch-Johnson, J., Wang, J., McInerney, D., & Moyer, E. J. (2021). Changes in future precipitation mean and variability across scales. *Journal of Climate*, *34*(7), 2741–2758. doi: 10.1175/JCLI-D-20-0001.1

Seeley, J. T., & Romps, D. M. (2015). Why does tropical Convective Available Potential Energy (CAPE) increase with warming? *Geophysical Research Letters*, *42*(23), 10,429-10,437. doi: 10.1002/2015GL066199

Singh, M. S., & O'Gorman, P. A. (2013). Influence of entrainment on the thermal stratification in simulations of Radiative-Convective Equilibrium. *Geophysical Research Letters*, *40*(16), 4398–4403. doi: 10.1002/grl.50796

Singh, M. S., & O'Gorman, P. A. (2015). Increases in moist-convective updraught velocities with warming in Radiative-Convective Equilibrium: Increases in updraught velocities with warming. *Quarterly Journal of the Royal Meteorological Society*, *141*(692), 2828–2838. doi: 10.1002/qj.2567

Sun, X., Xue, M., Brotzge, J., McPherson, R. A., Hu, X.-M., & Yang, X.-Q. (2016). An evaluation of dynamical downscaling of central plains summer precipitation using a WRF-based regional climate model at a convection-permitting 4 km resolution. *Journal of Geophysical Research: Atmospheres*, *121*(23), 13,801–13,825. doi: 10.1002/2016JD024796

Trapp, R. J., Diffenbaugh, N. S., & Gluhovsky, A. (2009). Transient response of severe thunderstorm forcing to elevated greenhouse gas concentrations. *Geophysical Research Letters*, *36*(1). doi: 10.1029/2008GL036203

Wang, Z., Franke, J. A., Luo, Z., & Moyer, E. J. (2021). Reanalyses and a high-resolution model fail to capture the "high tail" of CAPE distributions. *Journal of Climate*, *34*(21), 8699–8715. doi: 10.1175/JCLI-D-20-0278.1

Williams, E., & Renno, N. (1993, 01). An analysis of the conditional instability of the tropical atmosphere. *Monthly Weather Review*, *121*(1), 21-36. doi: 10.1175/1520-0493(1993)121⟨0021:AAOTCI⟩2.0.CO;2

Ye, B., Del Genio, A. D., & Lo, K. K.-W. (1998). CAPE variations in the current climate and in a climate change. *Journal of Climate*, *11*(8), 1997-2015. doi: 10.1175/1520-0442-11.8.1997

Zhang, Y., & Boos, W. R. (2023). An upper bound for extreme temperatures over midlatitude land. *Proceedings of the National Academy of Sciences*, *120*(12), e2215278120. doi: 10.1073/pnas.2215278120

Zhou, W., & Xie, S.-P. (2019). A conceptual spectral plume model for understanding tropical temperature profile and convective updraft velocities. *J. Atmos. Sci.*, *76*(9), 2801–2814.

# Supporting Information for "Robust Relationship Between Midlatitudes CAPE and Moist Static Energy Surplus in Present and Future Simulations"

Ziwei Wang [1,2], Elisabeth J. Moyer [1,2]

[1]Department of the Geophysical Sciences, University of Chicago, Chicago, Illinois

[2]Center for Robust Decision-making on Climate and Energy Policy (RDCEP), University of Chicago, Chicago, Illinois

## Contents of this file



## Text S1. Derivation of CAPE-MSE surplus framework

In this section we show the background for the framework in our manuscript. We repeat the derivation from Emanuel, *Atmospheric Convection* (1994) that restates CAPE as a function of pseudo-entropy, show how this can be approximated as a linear dependence in pseudo-enthalpy (moist static energy), and finally demonstrate that the error introduced by the core assumption required in Emanuel (1994) (hereafter E94) – that virtual temperature corrections can be ignored – is relatively minor and considerably smaller than that in an alternative CAPE framework.

*Emanuel (1994) derivation*

We start from the definition of CAPE in pressure coordinates:

$$CAPE = \int_{p_n}^{p_i} (\alpha_p - \alpha_a) dp \tag{1}$$

where $\alpha_p$ and $\alpha_a$ are the volume per mass for air in the parcel and the environment, respectively. Because CAPE is a positive quantity, the integration is from low to high pressure, i.e. from the top of a convective event ($p_n$) to the level of convective initiation ($p_i$).

The rising parcel will be saturated, and changes in its volume per mass can be divided into two terms, separating the effects of its saturation pseudo-entropy $s^*$ (which is independent of moisture) and of its actual moisture content. That is:

$$\Delta\alpha = \left.\frac{\partial\alpha}{\partial s^*}\right|_r \Delta s^* + \left.\frac{\partial\alpha}{\partial r}\right|_{s^*} \Delta r \tag{2}$$

If we treat the environment as also saturated – acceptable if the effect of moisture on density is small – then it can be similarly decomposed and CAPE can be written as:

$$CAPE = \int_{p_n}^{p_i} \left( \frac{\partial\alpha}{\partial s^*}(s_p^* - s_a^*) + \frac{\partial\alpha}{\partial r}(r_p - r_a) \right) \cdot dp \tag{3}$$

The volume per mass of dry air ($\alpha_d$) can be approximated as $\alpha_d = \frac{\alpha}{1+r}$. where $r$ is the mass mixing ratio of water vapor, typically 0.01 or less. Emanuel then makes the further assumption that the buoyancy effects of this water vapor $r$ (the virtual temperature effect) can be neglected entirely, so that the second term in Equation (3) vanishes and in the first term $\alpha$ is replaced by $\alpha_d$. This yields Eq. (6.4.2a) in Emanuel (1994):

$$CAPE \approx \int_{p_n}^{p_i} \frac{\partial\alpha_d}{\partial s^*}(s_p^* - s_a^*) \cdot dp \tag{4}$$

The neglect of virtual temperature effects for both parcel and environment produces a slight net underestimation of derived CAPE, but the distortion is smaller than in other approximate CAPE frameworks and is compensated for by the empirical regression coefficient. See discussion at the end of the section and Figure S1. The Maxwell relationship $(\frac{\partial\alpha}{\partial s})_p = (\frac{\partial T}{\partial p})_s$ allows converting the integration coordinate in Equation (4) from pressure to temperature:

$$CAPE = \int_{p_n}^{p_i} \frac{\partial T}{\partial p}(s_p^* - s_a^*) \cdot dp \tag{5}$$

$$= \int_{T_n}^{T_i} (s_p^* - s_a^*) \cdot dT \tag{6}$$

which is Equation (6.4.2) in Emanuel (1994).

Because the integration is now over temperature, and the difference between environment and parcel is taken at the same $T$, we can readily substitute saturated pseudo-enthalpy $h^*$ for the saturated pseudo-entropy $s^*$ via:

$$\Delta h^* = T\Delta s* \tag{7}$$

Equation (6) then becomes:

$$CAPE = \int_{T_n}^{T_i} \frac{h_p^* - h_a^*}{T} dT \tag{8}$$

Here $h_p^* = h_s$ is conserved for an adiabatically rising parcel, while the moist static energy of the environment $h_a^*$ is a weak function of $T$ in individual atmospheric profiles, reaching a minimum in mid-troposphere that can be $<$15% below $h_s$.

*Approximating the integral as a simple difference*

All simplified frameworks for CAPE must replace the integral with some kind of simple difference. If the moist static energy difference between the parcel and the environment were independent of $T$, we could write

$$CAPE = (h_s - \overline{h^*}) \cdot ln\frac{T_i}{T_n} \tag{9}$$

This assumption is obviously not realistic and in practice the true shape of atmospheric profiles necessitates adding an empirical coefficient to the relationship. Since an empirical coefficient is needed regardless, for convenience we take the difference at the location of the minimum tropospheric MSE, typically around 650 mb.

$$CAPE \approx A \cdot (h_s - h_m^*) \tag{10}$$

which is the linear relationship used in this work; $(h_s - h_m^*)$ is the " MSE surplus". The coefficient A captures the shape of the profile, and, if virtual temperature corrections were indeed negligible, would be mathematically constrained to be between zero and $ln\frac{T_i}{T_n}$ (see also Agard and Emanuel (2017)), at maximum $\sim$0.4 (for $T_i = 300$ K, $T_n = 200$ K). (In practice, compensating for the neglected virtual temperature corrections raises $A$ slightly.) For the same temperature range, a larger $A$ corresponds to a more uniform $\Delta h$ profile between the lifting condensation level and the tropopause. For the dataset used in this work, the empirical slope $A$ is 0.27.

*Effect of assumptions in derivation*

The derivation in E94 relies on two successive assumptions about the direct effect of water on the density of the environment through which a parcel rises. We show here that the effect of these assumptions is not prohibitive and is smaller than the effect of the core assumption in the alternative CAPE framework of Eq. (5) in Li and Chavas (2021) (LC21). The assumptions are:

- E94a: compute the virtual temperature effect for the environment assuming saturation
- E94b: neglect the virtual temperature effect for both parcel and environment
- LC21 Equation (5): assume all water vapor in the parcel condenses at the LCL

In reality, the mean environmental relative humidity in our high-CAPE midlatitudes summertime profiles is 0.44 (for all levels below 200 hPa). Both of the assumptions in E94 will therefore produce an underestimation of CAPE (the parcel is less buoyant than in reality), while that in LC21 will produce an overestimation (the parcel is more buoyant).

We illustrate the effects of these assumptions on an example atmospheric profile in Figure S1. The example profile is chosen to match the location and time of Figure 3 in Li and Chavas (2021): Springfield, MO in early June. At 650 hPa, the true buoyancy $g\frac{\Delta T_v}{T_{ve}}$ is 0.143 $m/s^2$. The assumptions in E94 underestimate buoyancy by 14% and 22% (0.123 and 0.111 $m/s^2$), while that in LC21 overestimates it by a factor of 6 (0.845 $m/s^2$). The discrepancies are about half as large when averaged over the parcel's ascent but their relative sizes are unchanged: E94a,b cause underestimations of 6% and 7% and LC21 causes an overestimation of a factor of 3. If we use instead an average summertime profile over the Southeastern U.S., the bias produced by E94 remains below 13% while that in LC21 is a factor of eight. In both frameworks, the bias is largely accounted for by an empirical regression coefficient, but the more modest assumptions of E94 lead to a robust regression across climate states.

**References**

Agard, V., & Emanuel, K. (2017). Clausius–Clapeyron scaling of peak CAPE in continental convective storm environments. *Journal of the Atmospheric Sciences*, *74*(9), 3043–3054.

Emanuel, K. (1994). Atmospheric Convection, Chap. 6. In (pp. 169–175). Oxford Univ. Press.

Li, F., & Chavas, D. R. (2021). Midlatitude continental CAPE is predictable from large-scale environmental parameters. *Geophysical Research Letters*, *48*(8), e2020GL091799.

# Figures S1 – S9

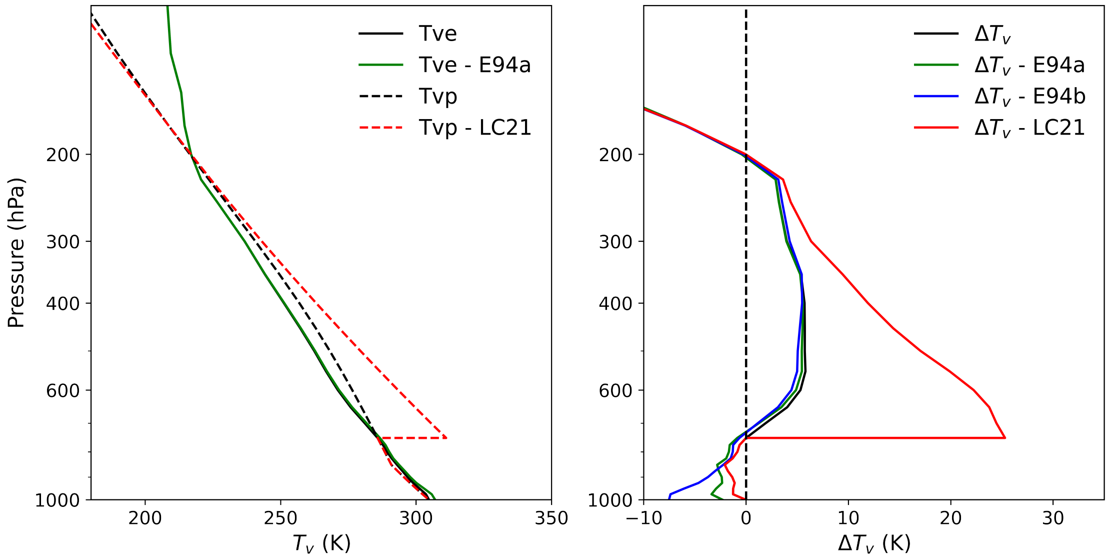


**Figure S1.** Illustration of the effect of assumptions in E94 and LC21, on (left) the virtual temperatures of parcel and environment and (right) the virtual temperature difference between parcel and environment. The example profile is that for a 1 × 1 deg grid in ERA5 including Springfield, MO, at 18 UTC on June 6th, 2005, chosen to approximately match the snapshot used in LC21 Figure 3 (0000 UTC June 07, 2011). E94a (green) raises the environmental $T_v$; E94b (blue) lowers $T_v$ in both environment and parcel; and LC21 (red) raises $T_v$ in the parcel by condensing all water at the LCL. The biases introduced by E94 are more modest than those in LC21, though all are ultimately accounted for by empirical regression coefficients.

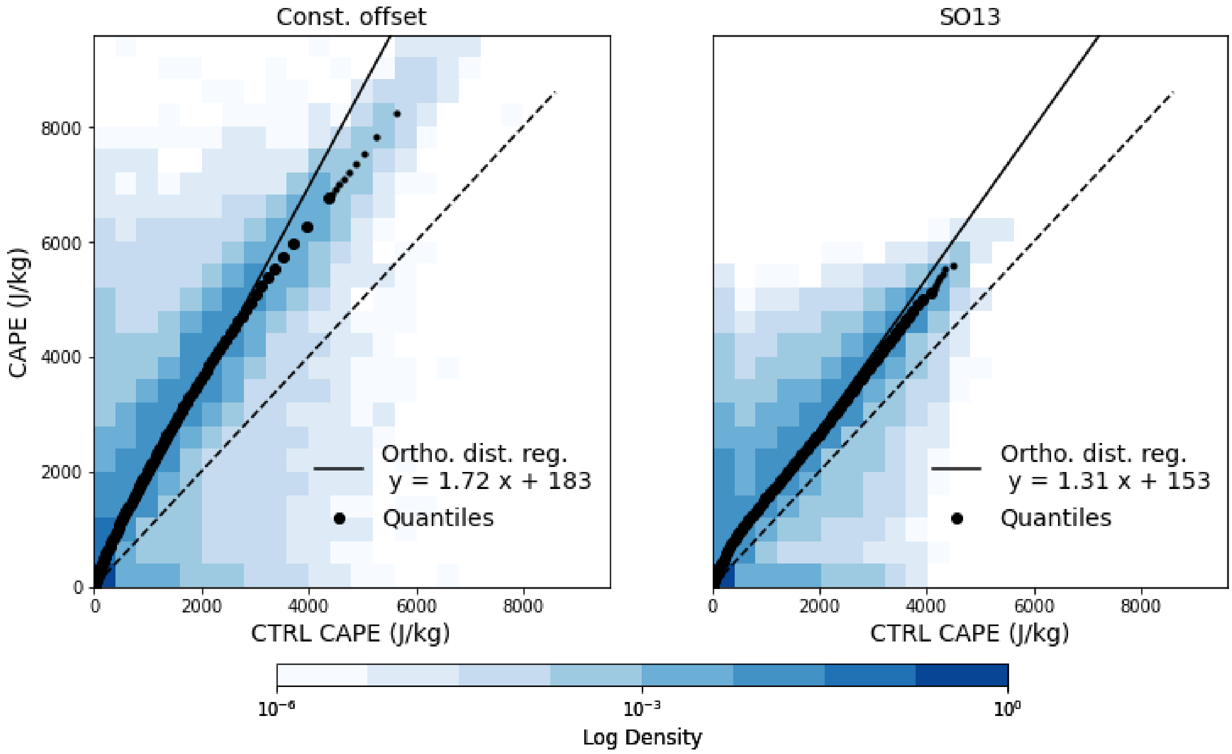


**Figure S2.** Changes between present and future CAPE, as in main text Figure 1 left panel, but for (left) *constant-offset* and (right) *SO13*, calculated as described in text. CAPE changes are too large in *constant offset* and too small in *SO13*: dividing by 4.65 K produces fractional changes of 12%/K and 6%/K, respectively, vs. the 8%/K derived from model output. For *constant offset* in particular, the quantiles fall below the orthogonal distance regression line above the 80th percentile. In both cases, however, the quantile regression matches the orthogonal distance regression reasonably well.

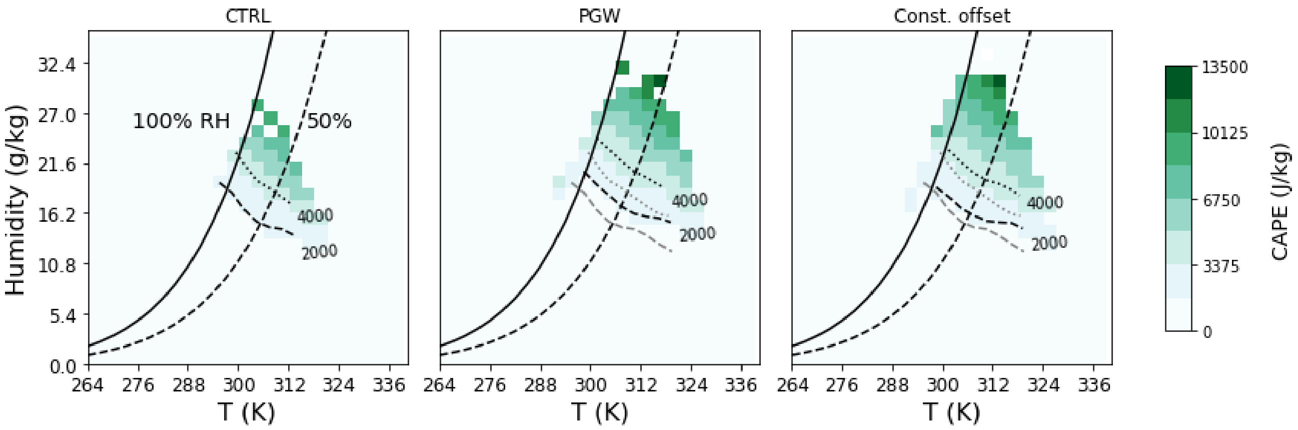


**Figure S3.** (Left and middle) Mean CAPE heatmap as in main text Figure 2 for present and future model output and (right) for the *constant offset* synthetic representation of future CAPE. Contours in black show CAPE of 2000 and 4000 J/kg in each panel, with CTRL contours repeated in gray in middle and right panels. Contours shift in PGW model output (center), meaning that warmer or wetter conditions are required to achieve the same CAPE. The *constant offset* synthetic (right), which involves changes in surface conditions alone and has no lapse rate adjustment, exhibits about half the shift of the PGW simulations.

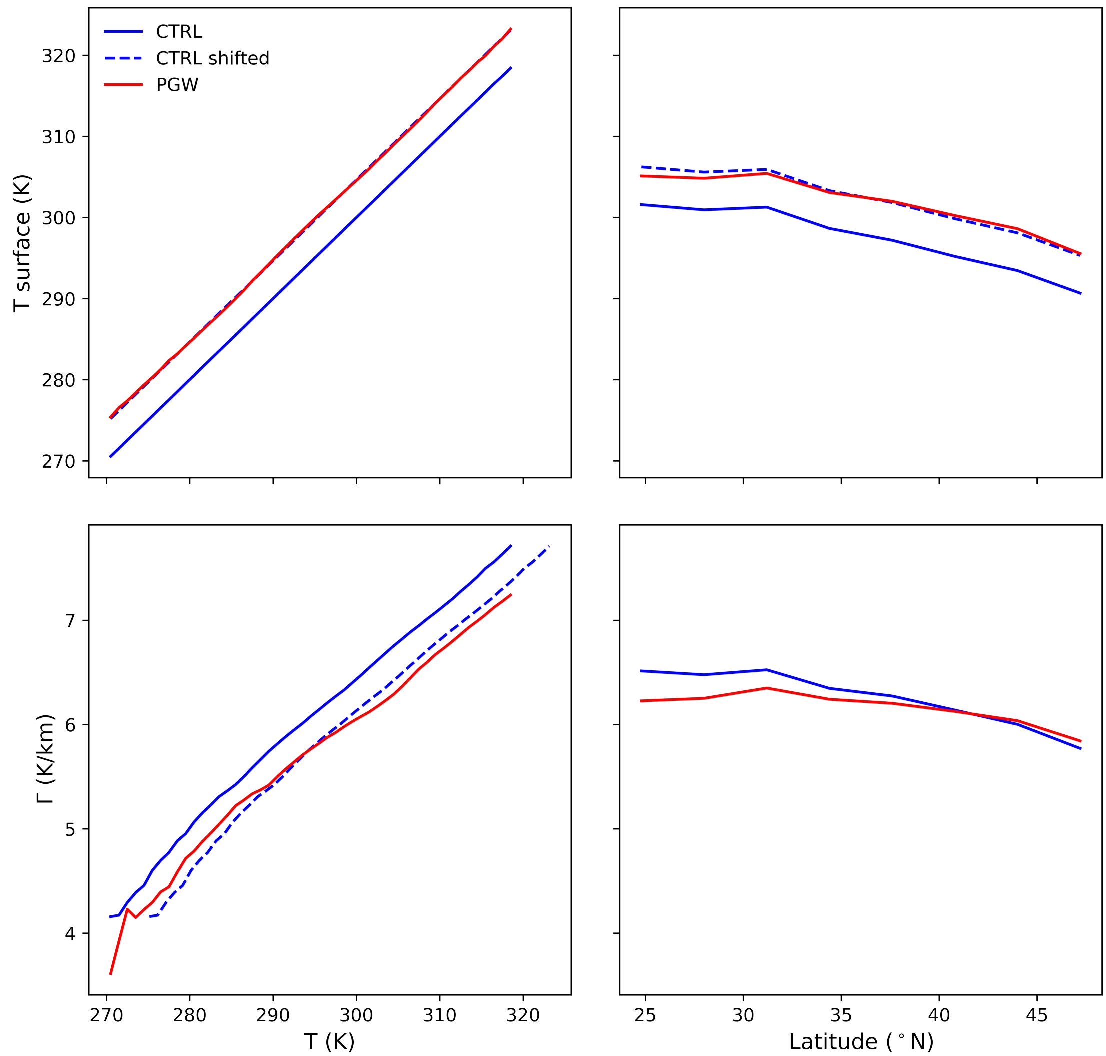


**Figure S4.** Changes in (top) temperature and (bottom) lapse rate as a function of (left) temperature bins and (right) latitudinal bins. The blue dashed lines are synthetics applying a same 4.65 K offset to the CTRL climate (blue solid lines). The damping of CAPE under a warmer climate can be explained by a more stable lapse rate associated with a set of given surface conditions.

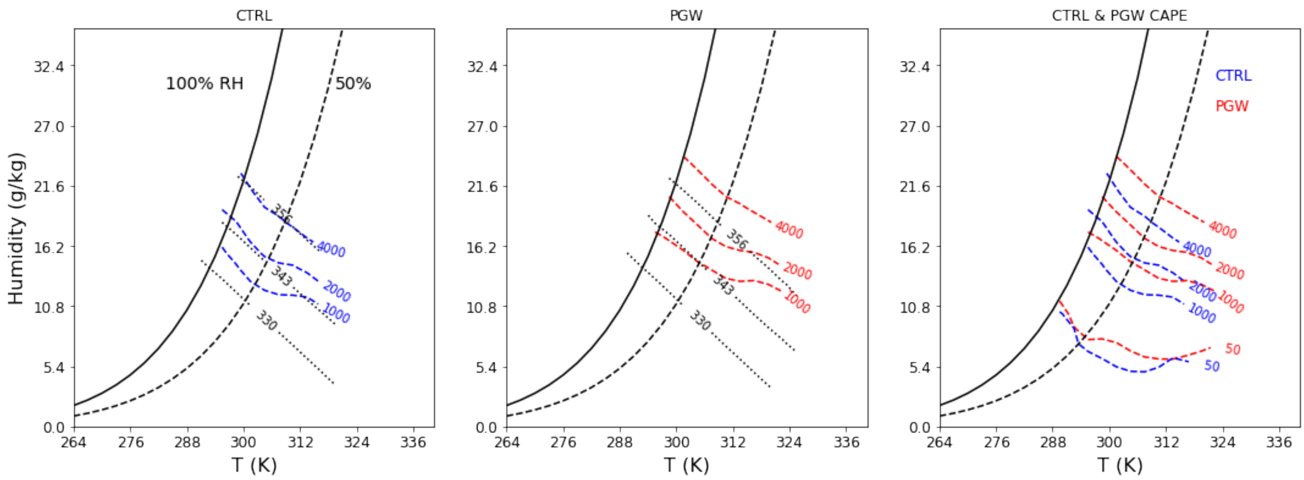


**Figure S5.** Contours of CAPE and surface moist static energy (MSE) in model output for simulations in present (CTRL, left) and future (PGW, middle) conditions. CAPE contours follow those of moist static energy in the convection-promoting regime (CAPE $>$ 1000 J/kg, RH $>$ 40%), The relationship differs between CTRL and PGW (right). Contours here are cut off at RH=100%, as in main text Figure 2. CAPE contours aligns with those of surface MSE in conditions with high CAPE, suggesting a strong dependence between CAPE and surface MSE. Future changes in CAPE can be translated to a change in mapping between surface MSE and CAPE.

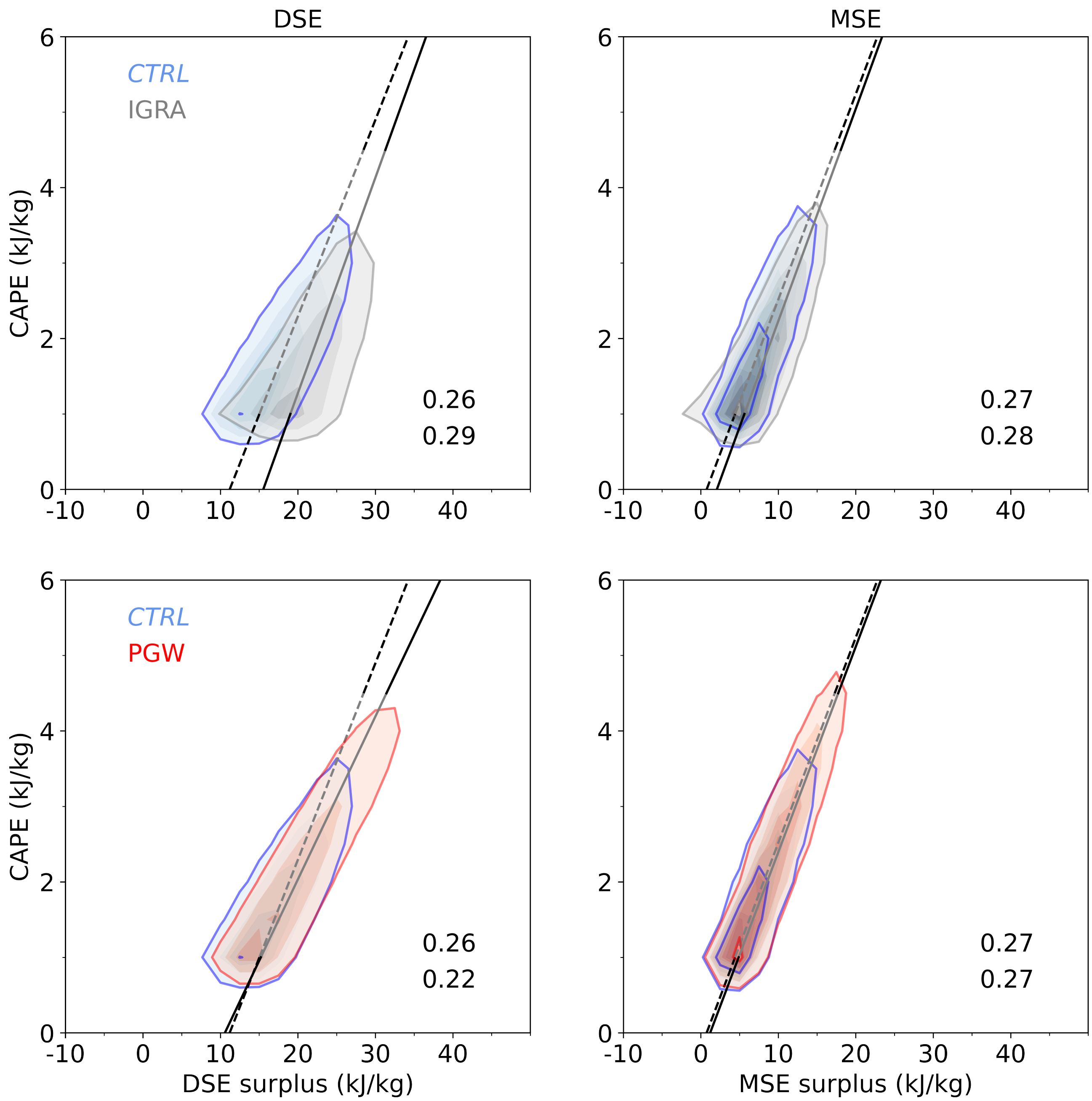


**Figure S6.** Comparison of the CAPE relationship with dry static energy (DSE) surplus (left) and with MSE surplus (right). DSE surplus is defined as the difference between surface MSE and mean mid-tropospheric DSE (virtual-temperature weighted free troposphere DSE). The top rows show model output (WRF) versus observations (IGRA) under CTRL climate, and the bottom rows show CTRL versus PGW in model output. Color shading increments are 1.5% for all panels, and the text shows the slopes for CTRL and IGRA/PGW. Conclusions are 1) the WRF simulation realistically reproduces the observed joint distribution of CAPE and MSE surplus and 2) a linear expression with MSE surplus outperforms that with DSE surplus both in residual variance and in robustness.

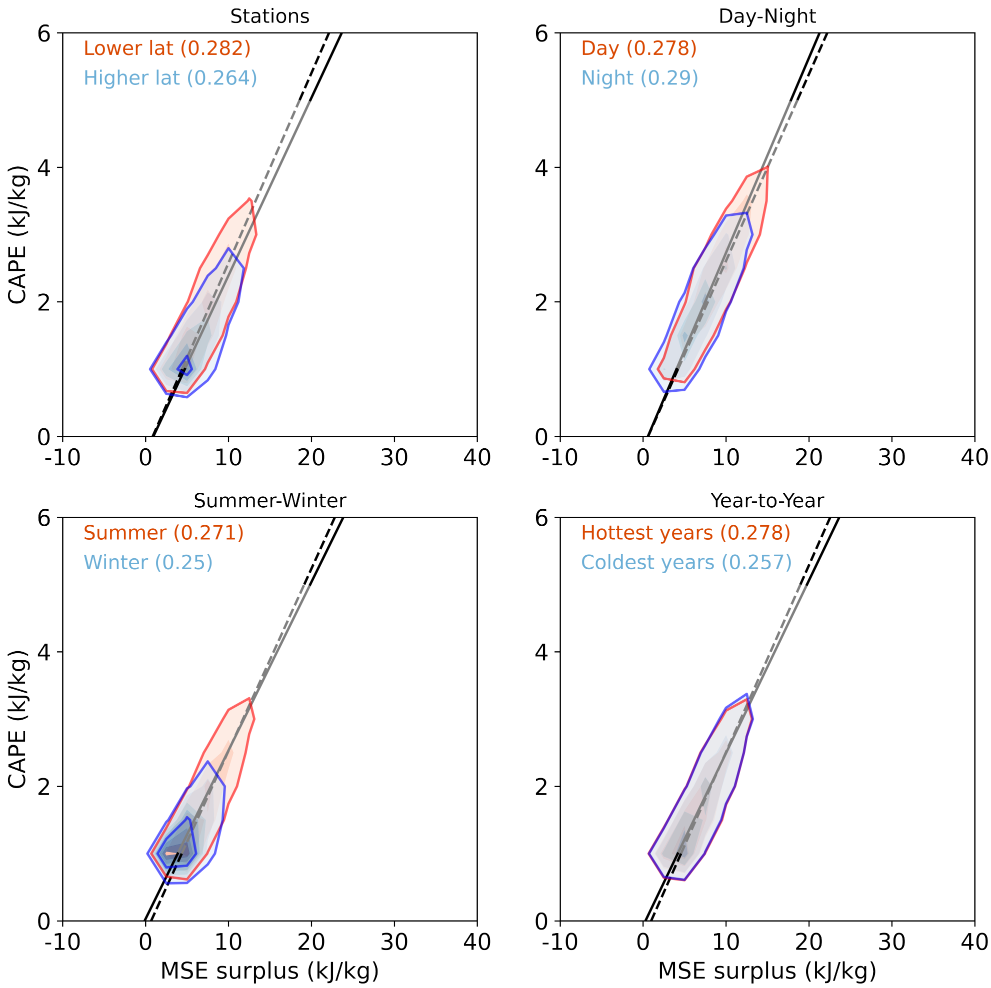


**Figure S7.** Tests of the robustness of the CAPE-MSE surplus relationship with different subsets of the data. *Top left*: stations lower and higher latitude than 35N. *Top right*: daytime versus nighttime (using only stations below 30N, to avoid biasing the sampling). *Bottom left*: summertime (MJJA) versus wintertime (NDJF) (all other panels use summertime data only; note that the month of February 2005 in the PGW run is removed due to missing surface 2D fields). *Bottom right*: the hottest 3 years (2001, 2006, 2012) versus the coldest 3 years (2004, 2008, 2009). Figure uses only CAPE $\geq$ 1000 J/kg, and all panels besides lower L. use summertime data only. MSE surplus is derived using the minimum saturation MSE in each individual profile. Each color shading is a 1.5% increment in density, and the orthogonal regression is fit using binned median values. The CAPE-MSE surplus framework (including its intercepts and slopes) is highly consistent across all cases tested.

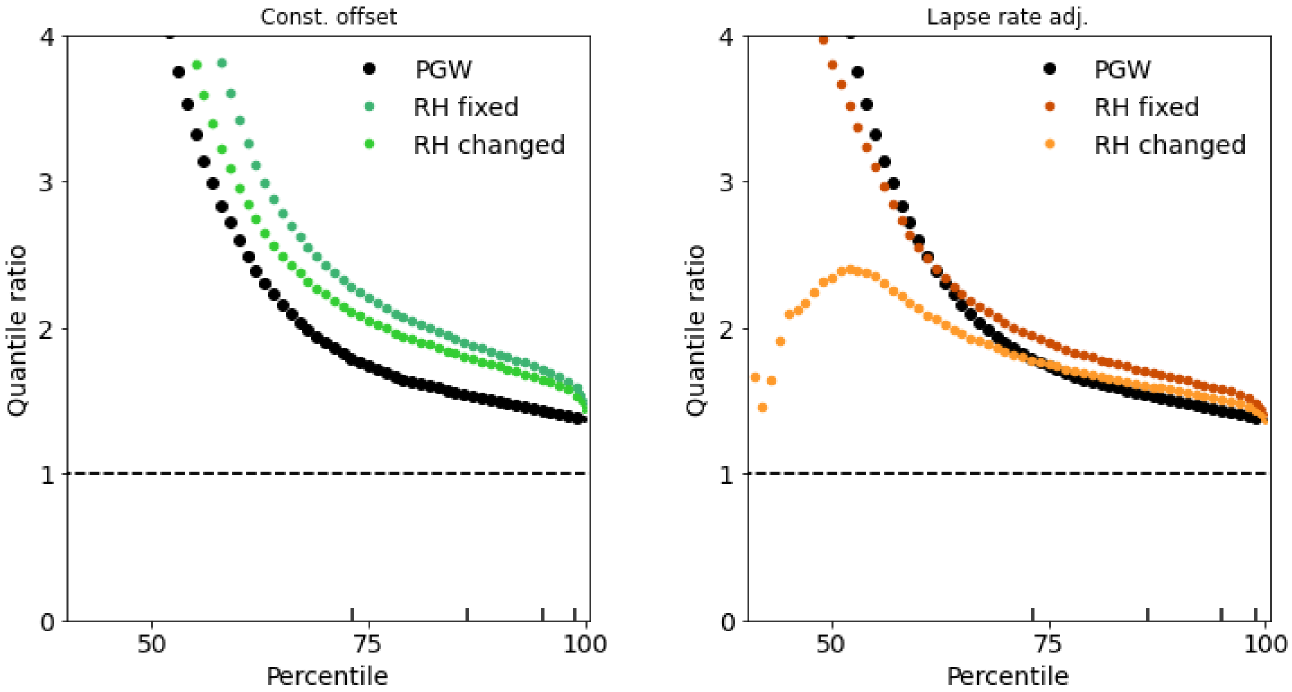


**Figure S8.** Quantile ratio plots of future–present CAPE in model output (PGW vs. CTRL) and in synthetic future distributions, showing also the effect of RH changes. For each synthetic we show one version with constant surface RH and one with a uniform $\sim$1% reduction, which lowers future CAPE changes by about 6% in both cases. (Left) *Constant offset*. Mean fractional changes are 1.92 with fixed RH and 1.81 with the reduction. Values are derived from the average quantile ratios for $\geq$ 73rd percentile. (Right) *Lapse rate adjustment*. Mean fractional changes are 1.71 and 1.61.

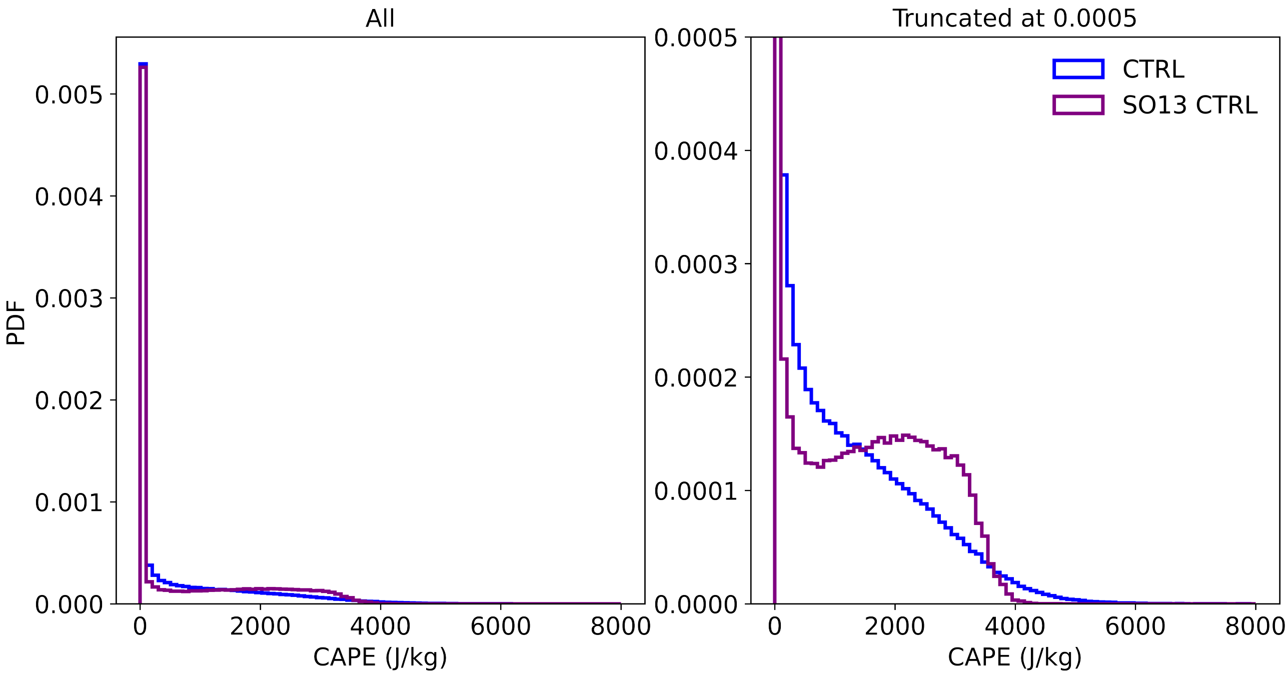


**Figure S9.** Comparison of probability distributions of midlatitdues summertime CAPE under current CTRL climate in our WRF model output and in the SO13 zero-buoyancy model driven by CTRL surface temperatures. (Left) full CAPE distribution and (right) with y-axis truncated at 0.0005 to show detail. The zero-buoyancy model cannot reproduce a realistic distribution, overestimating the occurrence of moderately high CAPE (between 1500 and 3500 J/kg). This peak occurs even though we modify the SO13 procedure to force the integration to stop at the actual LNB of each profile. Without that modification, SO13 cannot produce zero-CAPE values and the distribution is even more unimodal. SO13 is designed to reproduce climatological means in strongly convecting regions and is not appropriate for midlatitudes land.

# Tables S1 – S2

**Table S1.** List of CMIP6 Models included in this study and shown in main text Figure 3. The outputs are 6-hourly model level data, for both *historical* and *ssp585* experiments. All model output is available from ESGF (`https://esgf-node.llnl.gov/search/cmip6/`).

| Model | Variant label | Horizontal grid | Vertical levels |
|---|---|---|---|
| ACCESS-ESM1-5 | r6i1p1f1 | $192 \times 145$ | 38 |
| CanESM5 | r1i1p2f1 | $128 \times 64$ | 49 |
| CMCC-CM2-SR5 | r1i1p1f1 | $288 \times 192$ | 30 |
| CNRM-CM6-1 | r1i1p1f2 | $256 \times 128$ | 91 |
| CNRM-ESM2-1 | r1i1p1f2 | $256 \times 128$ | 91 |
| EC-Earth3 | r1i1p1f1 | $512 \times 256$ | 91 |
| GISS-E2-1-G | r1i1p1f2 | $144 \times 90$ | 40 |
| MIROC-ES2L | r1i1p1f2 | $128 \times 64$ | 40 |
| MPI-ESM1-2-LR | r1i1p1f1 | $192 \times 96$ | 47 |
| MPI-ESM1-2-HR | r1i1p1f1 | $384 \times 192$ | 95 |
| NorESM2-MM | r1i1p1f1 | $288 \times 192$ | 32 |

**Table S2.** Evaluating synthetics: fitted slopes and intercepts of the future CAPE-MSE framework as in main text Figure 4, for actual PGW model output and for three synthetic datasets. *C–C* scaling produces too small a slope and *constant offset* too small an intercept. *Lapse rate adjustment* performs well at both.

| | PGW | C–C | Constant offset | Lapse rate adj. |
|---|---|---|---|---|
| slope | 0.239 | 0.271 | 0.240 | 0.236 |
| x-intercept (kJ/kg) | 346.2 | 350.4 | 343.8 | 345.8 |